Accounting for conformational flexibility and torsional anharmonicity in the H + CH3CH2OH hydrogen abstraction reactions: A multi-path variational transition state theory study

Rubén Meana-Pañeda and Antonio Fernández-Ramos

Citation: The Journal of Chemical Physics **140**, 174303 (2014); doi: 10.1063/1.4873350
View online: http://dx.doi.org/10.1063/1.4873350
View Table of Contents: http://scitation.aip.org/content/aip/journal/jcp/140/17?ver=pdfcov
Published by the AIP Publishing

Accounting for conformational flexibility and torsional anharmonicity in the H + CH_3CH_2OH hydrogen abstraction reactions: A multi-path variational transition state theory study

Rubén Meana-Pañeda[a] and Antonio Fernández-Ramos[b]
Department of Physical Chemistry and Center for Research in Biological Chemistry and Molecular Materials, University of Santiago de Compostela, 15706 Santiago de Compostela, Spain

(Received 25 November 2013; accepted 15 April 2014; published online 6 May 2014)

This work reports a detailed theoretical study of the hydrogen abstraction reactions from ethanol by atomic hydrogen. The calculated thermal rate constants take into account torsional anharmonicity and conformational flexibility, in addition to the variational and tunneling effects. Specifically, the kinetics calculations were performed by using multi-path canonical variational transition state theory with least-action path tunneling corrections, to which we have added the two-dimensional non-separable method to take into account torsional anharmonicity. The multi-path thermal rate constant is expressed as a sum over conformational reaction channels. Each of these channels includes all the transition states that can be reached by internal rotations. The results show that, in the interval of temperatures between 250 and 2500 K, the account for multiple paths leads to higher thermal rate constants with respect to the single path approach, mainly at low and at high temperatures. In addition, torsional anharmonicity enhances the slope of the Arrhenius plot in this range of temperatures. Finally, we show that the incorporation of tunneling into the hydrogen abstraction reactions substantially changes the contribution of each of the transition states to the conformational reaction channel. © *2014 AIP Publishing LLC*. [http://dx.doi.org/10.1063/1.4873350]

I. INTRODUCTION

One of the key steps in the decomposition and combustion of ethanol is the hydrogen abstraction by atomic hydrogen[1–4] through the three following pathways:

$$CH_3CH_2OH + H \rightarrow CH_3CHOH + H_2, \quad \text{(R1)}$$

$$CH_3CH_2OH + H \rightarrow CH_2CH_2OH + H_2, \quad \text{(R2)}$$

$$CH_3CH_2OH + H \rightarrow CH_3CH_2O + H_2. \quad \text{(R3)}$$

Norton and Dryer[1] pointed out the importance of including the three channels in the study of the mechanisms for ethanol oxidation, as well as the relevance of knowing the proportions of each of the three radicals since they lead to different products. The total hydrogen abstraction thermal rate constants have been measured by Aders and Wagner[5] at temperatures between 295 and 700 K, whereas reaction (R1) has been measured by Bansal and Freeman[6] at $T = 423$ K from γ radiolysis of ethanol vapor. However, from the experimental point of view the individual thermal rate constants for (R1), (R2), and (R3) and therefore the branching ratios are difficult to determine. Probably, the best estimate is a computational study carried out by Park *et al.*,[7] although these authors introduce some approximations which may affect the accuracy of the calculated thermal rate constants. For instance, they considered only the most stable conformer for each of the reactions, but both ethanol and the transition states of reactions (R1), (R2), and (R3) present several conformers that can be reached by rotation about single bonds. A reaction involving multiple conformations differs from that with a single conformation, because the former has conformational flexibility with low barriers of interconversion between conformers and with several transition states that can lead to different conformations of the same products.

It is the objective of this work to study reactions (R1), (R2), and (R3) taking into account all the possible conformers relevant to the reactive processes. We also describe a methodology than can deal with both torsional anharmonicity and the increase of the reactivity due to the incorporation of multiple transition states (or multiple paths) into the reaction. These are two issues that require careful consideration and that will be present in all combustion reactions involving flexible molecules. Another interesting issue that we discuss in this study is how well conventional transition state theory (TST)[8] accounts for the contribution of each of the transition states to the rate constant.

The total forward thermal rate constant for the hydrogen abstraction from ethanol is a sum over all the transition states or, similarly, over the reaction paths,[9] which are individually calculated using variational transition state theory (VTST).[10,11] This methodology is called multi-path variational transition state theory (MP-VTST),[9,12,13] to distinguish it from single-path VTST. It can be invoked when the internal torsions are treated within the harmonic approximation[9] or within some specific anharmonic treatment.[12,13] Specifically, for the three reactions, (R1), (R2), and (R3), we have used the two-dimensional non-separable (2D-NS) method,[14] which

[a]Current address: Department of Chemistry, University of Minnesota, 207 Pleasant Street SE, Minneapolis, Minnesota 55455-0431, USA.
[b]Electronic mail: qf.ramos@usc.es

allows an accurate calculation of hindered rotor partition functions. Other methods that could be used for the calculation of torsional anharmonicity for more than one hindered rotor without invoking separability between the torsions are: the torsional path integral Monte Carlo method;[15–18] the multi-structural method with a coupled torsional potential;[19] and the extended hindered-rotor model.[20] In the 2D-NS method, the two-dimensional torsional potential of the molecule is fitted to Fourier series. With this analytical potential it is possible to solve the Schrödinger equation by the variational method and to calculate the quantum two-dimensional partition function. The resulting partition function is incorporated into the total rovibrational partition function, as described in Sec. II.

We also propose a convenient way of expressing the MP-VTST thermal rate constant, i.e., as a sum over what we call conformational reaction channels (CRC). Each of these channels is given by all the transition state structures that can be reached by internal rotations. These issues are described in Sec. II, whereas the analysis about the relevance of tunneling, anharmonicity, and conformational flexibility, for the hydrogen abstraction reactions is discussed in Sec. III.

II. METHODOLOGY

This section first describes how to incorporate the 2D-NS method for hindered rotors into the multi-conformer rovibrational partition function. Second, it shows how to implement this method, which takes into account the anharmonicity of the torsional modes, into the MP-VTST methodology.

A. The multi-conformer rovibrational partition function

The multi-conformer rovibrational partition function is built from the potential generated by all the conformers that can be reached by the scanned rotation of the torsional coordinates, but with the rest of the internal coordinates minimized at every point along this potential. It should be noticed that we call the partition function multi-conformational and not multi-structural,[21] because the former refers to a set of structures that can only be reached by internal rotation, whereas the latter does not necessarily involve structures which are interconvertible conformers. The number of conformers (distinguishable configurations) is given by the total number of minima of the torsional potential divided by the symmetry number of the internal rotations.[22] The multi-conformer rovibrational partition function, $\tilde{Q}_{\rm tor}$, is related to its harmonic counterpart by[14]

$$\tilde{Q}_{\rm tor} = \alpha_{\rm tor}\tilde{Q}_{\rm har}, \tag{1}$$

where $\alpha_{\rm tor}$ is the anharmonic coefficient calculated by the 2D-NS method, and $\tilde{Q}_{\rm har}$ is the total rigid-rotor harmonic-oscillator (RRHO) partition function of the conformers. The latter can be written as a sum over the rovibrational partition functions of the individual conformers

$$\tilde{Q}_{\rm har} = \sum_{i=1}^{n_{\rm C}} Q_i^{\rm RRHO} \tag{2}$$

being $n_{\rm C}$ the number of conformers. The RRHO partition function for each of the conformers is the product of the classical rigid-rotor rotational partition function $Q_{{\rm rot},i}$ and the $Q_i^{\rm HO}$ normal-mode harmonic oscillator quantum vibrational partition function, i.e.,

$$Q_i^{\rm RRHO} = Q_{{\rm rot},i}\,Q_i^{\rm HO}e^{-\beta U_i} \tag{3}$$

being $\beta = 1/k_BT$, k_B is the Boltzmann constant, and T is the temperature. The Boltzmann factor takes into account the difference in energy, U_i, between conformer i and the most stable conformer.

The coefficient $\alpha_{\rm tor}$ includes the correction to the multi-conformer harmonic partition function when torsions are calculated with the 2D-NS anharmonic treatment instead of with the harmonic approximation, i.e.,

$$\alpha_{\rm tor} = \frac{Q_{\rm tor}^{\rm 2D-NS}}{\overline{Q}_{\rm tor}^{\rm MC-HO}}. \tag{4}$$

The multi-conformer harmonic-oscillator partition function, $\overline{Q}_{\rm tor}^{\rm MC-HO}$, of Eq. (4) due to t torsions is given by

$$\overline{Q}_{\rm tor}^{\rm MC-HO} = \sum_{i=1}^{n_{\rm C}} e^{-\beta U_i}\prod_{\tau=1}^{t}\overline{q}_{i,\tau}^{\rm HO} \tag{5}$$

being

$$\overline{q}_{\tau}^{\rm HO} = \frac{e^{-\beta\hbar\overline{\omega}_\tau/2}}{1-e^{-\beta\hbar\overline{\omega}_\tau}}. \tag{6}$$

If $t = 2$, the two torsional frequencies $\overline{\omega}_{i,\tau}$, $(\tau = 1, 2)$ of minimum i are obtained from the roots of the 2×2 secular determinant

$$|\mathbf{K}_i - \overline{\omega}_{i,\tau}\mathbf{D}_i| = 0 \tag{7}$$

being

$$\mathbf{K}_i = \begin{pmatrix} \frac{\partial^2 V}{\partial\phi_1^2} & \frac{\partial^2 V}{\partial\phi_1\partial\phi_2} \\ \frac{\partial^2 V}{\partial\phi_1\partial\phi_2} & \frac{\partial^2 V}{\partial\phi_2^2} \end{pmatrix} \tag{8}$$

the torsional force constants matrix, with the derivatives evaluated at the equilibrium position of conformer i, and

$$\mathbf{D}_{\rm i} = \begin{pmatrix} I_{i,1} & -\Lambda_{i,12} \\ -\Lambda_{i,12} & I_{i,2} \end{pmatrix} \tag{9}$$

the reduced $\mathbf{D}$ matrix.[23] The two reduced moments of inertia $I_{i,\tau}$ $(\tau = 1, 2)$ are calculated at the geometry of minimum i, and $\Lambda_{i,12}$ is the coupling between them. See Ref. 14 for further details.

The potential and the second derivatives of the potential are obtained from a fit to Fourier series of the type

$$V_{\rm tor}(\phi_1,\phi_2) = V_1(\phi_1) + V_2(\phi_2) + \sum_{L_1=1}^{L_{1,\max}}\sum_{L_2=1}^{L_{2,\max}} c_{L_1L_2}\cos(L_1\phi_1)\cos(L_2\phi_2) + \sum_{P_1=1}^{P_{1,\max}}\sum_{P_2=1}^{P_{2,\max}} d_{P_1P_2}\sin(P_1\phi_1)\sin(P_2\phi_2)$$

$$+\sum_{L'_1=1}^{L'_{1,\max}}\sum_{L'_2=1}^{L'_{2,\max}} c'_{L'_1L'_2}\cos(L'_1\phi_1)\sin(L'_2\phi_2)$$

$$+\sum_{P'_1=1}^{P'_{1,\max}}\sum_{P'_2=1}^{P'_{2,\max}} d'_{P'_1P'_2}\sin(P'_1\phi_1)\cos(P'_2\phi_2), \quad (10)$$

where $c_{L_1L_2}$, $L_1 = 1, \ldots, L_{1,\max}$, $L_2 = 1, \ldots, L_{2,\max}$, $d_{P_1P_2}$, $P_1 = 1, \ldots, P_{1,\max}$, $P_2 = 1, \ldots, P_{2,\max}$, $c'_{L'_1L'_2}$, $d'_{L'_1L'_2}$, $L'_1 = 1, \ldots, L'_{1,\max}$, $L'_2 = 1, \ldots, L'_{2,\max}$, and $d'_{P'_1P'_2}$, $P'_1 = 1, \ldots, P'_{1,\max}$, $P'_2 = 1, \ldots, P'_{2,\max}$ are fitting parameters, and $L_{1,\max}$, $L_{2,\max}$, $L'_{1,\max}$, $L'_{2,\max}$, $P_{1,\max}$, $P_{2,\max}$, $P'_{1,\max}$, and $P'_{2,\max}$ indicate the largest number of each series. The one-dimensional potentials are

$$V_1(\phi_1) = a_0 + \sum_{M=1}^{M_{\max}} a_M\cos(M\phi_1) + \sum_{M'=1}^{M'_{\max}} a'_{M'}\sin(M'\phi_1), \quad (11)$$

and

$$V_2(\phi_2) = b_0 + \sum_{N=1}^{N_{\max}} b_N\cos(N\phi_2) + \sum_{N'=1}^{N'_{\max}} b'_{N'}\sin(N'\phi_2), \quad (12)$$

where a_0, b_0, $a_M(M = 1, \ldots, M_{\max})$, $a'_{M'}(M' = 1, \ldots, M'_{\max})$, $b_N(N = 1, \ldots, N_{\max})$, $b'_{N'}(N' = 1, \ldots, N'_{\max})$ are fitting parameters, and $M_{\max}$, $M'_{\max}$, $N_{\max}$, and $N'_{\max}$ are the largest number of the coefficients of each series.

To calculate the 2D-NS partition function of Eq. (4), we have used a Hamiltonian of the form

$$H^{\text{2D-NS}} = \frac{-\hbar^2}{2}\left\{\frac{1}{I_1}\frac{\partial^2}{\partial\phi_1^2} + \frac{1}{I_2}\frac{\partial^2}{\partial\phi_2^2}\right\} + V_{\text{tor}}(\phi_1, \phi_2) \quad (13)$$

being $V_{\text{tor}}(\phi_1, \phi_2)$ the potential given by Eq. (10); and I_1 and I_2 the reduced moments of inertia of the absolute minimum of the torsional potential. It is not difficult to include coupling in the kinetic energy,[14,23] but we have found that in this case it has no effect in the resulting 2D-NS partition function, which is given by

$$Q_{\text{tor}}^{\text{2D-NS}} = \frac{1}{\sigma_{\text{tor}}}\sum_j e^{-\beta E_{\text{tor},j}} \quad (14)$$

being σ_{tor} the symmetry number associated to the torsions,[22] i.e., $\sigma_{\text{tor}} = \sigma_{\text{tor},1}\sigma_{\text{tor},2}$, and $E_{\text{tor},j}$ the calculated eigenvalues after the diagonalization of the Hamiltonian of Eq. (13). At high temperatures, this quantum partition function reduces to

$$Q_{\text{cl,tor}} = \frac{1}{\sigma_{\text{tor}}}\frac{(I_1I_2)^{1/2}}{2\pi\beta\hbar^2}\int_0^{2\pi}\int_0^{2\pi} d\phi_1 d\phi_2 e^{-\beta V(\phi_1,\phi_2)}, \quad (15)$$

which is the classical counterpart of Eq. (14).

B. The MP-VTST thermal rate constant

The thermal rate constant calculated by conventional TST[8] for a bimolecular reaction having only one equilibrium conformation of the reactants and one transition state is given by

$$k^{\text{TST}}(T) = B(T)\frac{Q_{\text{rot}}^{\ddagger}Q_{\text{vib}}^{\ddagger}}{Q_{\text{rot,R}}Q_{\text{vib,R}}} \quad (16)$$

being Q_{rot} and Q_{vib} the rotational and vibrational partition functions of the transition state ($\ddagger$) and of the reactants (R), respectively; the factor

$$B(T) = \frac{1}{h\beta}\frac{Q_{\text{e}}^{\ddagger}}{Q_{\text{e,R}}}\frac{1}{\Phi_{\text{rel}}}e^{-\beta V_0^{\ddagger}} \quad (17)$$

includes: the electronic partition functions (Q_e) of the transition state ($\ddagger$) and of the reactants (R); the partition function including the relative translational motion of the reactants, Φ_{rel}, which is one for unimolecular reactions; and the difference in energy, $V_0^{\ddagger}$, between the reactants and the transition state. The expression of Eq. (16) assumes that the transition state is the bottleneck for reaction and that there is no recrossing, i.e., those trajectories starting in the reactants side and that cross the dividing surface never return. Moreover, it is assumed that quantum effects are negligible. The canonical version of variational transition state theory with multidimensional tunneling corrections (CVT/MT)[10,11,24,25] incorporates a correction into these two approximations of TST through a multiplicative coefficient

$$k^{\text{CVT/MT}} = \gamma^{\text{CVT/MT}}(T)k^{\text{TST}}(T), \quad (18)$$

where

$$\gamma^{\text{CVT/MT}}(T) = \Gamma^{\text{CVT}}(T)\kappa^{\text{CVT/MT}}(T) \quad (19)$$

being $\Gamma^{\text{CVT}}(T)$ the coefficient that accounts for the recrossing (or variational effects), and $\kappa^{\text{CVT/MT}}(T)$ the transmission coefficient that accounts for quantum effects. The calculation of $\Gamma^{\text{CVT}}(T)$ involves placing several dividing surfaces along the minimum energy path. The CVT thermal rate constant, $k^{\text{CVT}}(T)$, is calculated at the dividing surface that maximizes the free energy of activation. Therefore, the recrossing coefficient is given by the ratio

$$\Gamma^{\text{CVT}}(T) = \frac{k^{\text{CVT}}(T)}{k^{\text{TST}}(T)} \quad (20)$$

and because $k^{\text{CVT}}(T) \le k^{\text{TST}}(T)$, then $\Gamma^{\text{CVT}}(T) \le 1$. The equality between the two thermal rate constants occurs only when the dividing surface is located at the transition state.

The TST and CVT thermal rate constants of Eq. (20) are sometimes called quasiclassical because quantum effects on the modes perpendicular to the reaction coordinate (being the reaction coordinate the normal mode with imaginary frequency at the transition state) are included by using quantum instead of classical vibrational partition functions. The effect is that the transmission coefficient, which accounts for the quantum nature of the reaction coordinate, is calculated over the vibrationally ground-state adiabatic potential, i.e., the classical plus zero-point-energy inclusive potential. In the CVT/MT theory, $\kappa^{\text{CVT/MT}}(T)$ is given by the ratio between semiclassical, $P^{\text{MT}}(E)$, and classical, $P^{\text{C}}(E)$, Boltzmann averaged transmission probabilities

$$\kappa^{\text{CVT/MT}}(T) = \frac{\int_0^{\infty} dE\, P^{\text{MT}}(E)\exp(-\beta E)}{\int_0^{\infty} dE\, P^{\text{C}}(E)\exp(-\beta E)}. \quad (21)$$

The classical transmission probability is zero below the potential, $V^*(T)$, at which the CVT dividing surface is located, and the unity above this potential. It is possible to integrate

the denominator of Eq. (21) to obtain

$$\kappa^{\mathrm{CVT/MT}}(T) = \beta \exp(\beta V^*(T)) \int_0^\infty dE\, P^{\mathrm{MT}}(E) \exp(-\beta E). \tag{22}$$

It should be noticed that $V^*(T)$ is temperature dependent because the location of the CVT dividing surface may change with temperature. For the calculation of the semiclassical transmission probabilities, the barrier height is given by the maximum of the vibrationally adiabatic potential, V^{AG}. Thus, at energies below V^{AG} the transmission probability is larger than zero if the molecules in the reactants side can penetrate through classically forbidden regions of the potential and reach products. This quantum effect is called tunneling and, in general, increases substantially the forward flux toward products (and therefore the rate constant) in reactions in which a light particle is being transferred. At energies above V^{AG} the transmission probability is smaller than unity due to non-classical reflection. Of the two quantum effects just mentioned, tunneling is usually the dominant effect in the transmission coefficient, so it is of common use to call $\kappa^{\mathrm{CVT/MT}}(T)$ tunneling transmission coefficient.

The evaluation of tunneling is not an easy task because of the multidimensional nature of the problem. The reaction coordinate is coupled to other degrees of freedom and this coupling affects the tunneling probabilities. One possibility is to select a few degrees of freedom and to treat them very accurately by quantum dynamics, as it has been done by Kerkeni and Clary[26,27] for some hydrogen abstraction reactions. Another possibility is to use a semiclassical approach, which is the methodology we follow in this study. Semiclassics is not as accurate as quantum dynamics, but allows us to include the coupling between the reaction coordinate and all the other degrees of freedom. In fact, VTST/MT has been tested against accurate quantum dynamics calculations for atom-diatom[28] and polyatomic reactions[29] with good results.

The coupling affects the tunneling path over which the tunneling probabilities are being calculated, i.e., the coupling curves the tunneling path to the concave side of the reaction path.[30] In the case of very large coupling the best tunneling path, at a given tunneling energy, would be close to a straight-line path (large curvature), whereas in the case of very weak coupling the best path would be close to the minimum energy path (small curvature). The small-curvature[31,32] and the large curvature tunneling approximations[33] can handle weak to intermediate and strong coupling, respectively. However, it is better to have a method that can search for the best tunneling path, i.e., a method that, at every tunneling energy, maximizes the tunneling probability (or similarly, a method that minimizes the imaginary action) without being restricted to a particular path. The least-action path tunneling (LAT) approximation,[34–36] that was recently developed for polyatomic reactions,[36–38] searches for the best tunneling path among several paths spanning from the minimum energy path to the straight-line path. Therefore, in this study we calculate the tunneling transmission coefficient using the LAT approximation. It is computationally more demanding than the small curvature and the large curvature approximations. However, LAT is more accurate than both of them, because it can handle reactions with all types of coupling.

The canonical variational transition state theory with least-action path tunneling corrections (CVT/LAT) with one reactant conformation and one transition state is given by

$$k^{\mathrm{CVT/LAT}}(T) = \gamma^{\mathrm{CVT/LAT}}(T) k^{\mathrm{TST}}(T). \tag{23}$$

Transition state theory assumes that the reactants are in quasiequilibrium with the transition state. If the reactants have a flexible structure that can lead to several conformers, the initial assumption of transition state theory still holds if each of the conformers of reactants are in equilibrium with each other. This occurs when all the barriers for interconversion between conformers are smaller than the barrier height for reaction. If the reaction has many conformers, the only difference with the TST of Eq. (16) is that the denominator is substituted by the multi-conformer rovibrational partition function of Eq. (2), if the rigid-rotor harmonic-oscillator is applied, or by the partition function of Eq. (1), if the two torsional modes are treated within the 2D-NS methodology.

Reactions with several reactant conformations usually present more than one transition state, so we need to account for all the transition states relevant to the reaction. This can be done using multi-path transition state theory (MP-TST), if we ignore recrossing and quantum effects, or by MP-VTST if we take them into account. These two theories, MP-TST and MP-VTST, are similar to conventional TST and to single-path VTST, respectively, with the additional assumption that the barriers of interconversion between the reactant conformations have to be smaller than the barrier heights of each of the transition states that lead to reaction. If the reaction has $n^\ddagger$ transition states (instead of just one transition state), the total MP-TST rate constant within the harmonic approximation is given by

$$k_{\mathrm{har}}^{\mathrm{MP-TST}}(T) = B(T) \sum_{i=1}^{n^\ddagger} \frac{Q_{\mathrm{rot},i}^\ddagger Q_i^{\mathrm{HO},\ddagger} e^{-\beta U_i^\ddagger}}{\tilde{Q}_{\mathrm{har,R}}} = B(T) \frac{\tilde{Q}_{\mathrm{har}}^\ddagger}{\tilde{Q}_{\mathrm{har,R}}}, \tag{24}$$

where $U_i^\ddagger$ is the difference in energy between transition state i and the transition state with the lowest energy. To obtain the rhs expression, we have used Eqs. (2) and (3). The barrier height of Eq. (17) included in $B(T)$ is calculated between the most stable reactant and the transition state with the lowest energy.

It is convenient to divide the $n^\ddagger$ transition states in sets of transition states belonging to a given reaction channel. Each of these channels is given by one multi-conformational partition function [see Eqs. (1) and (2)], i.e., each channel includes all the transition states that can be reached by rotation about the two torsions, so we call them CRCs. For a reaction with K conformational reaction channels ($k = 1, \ldots, K$), and each of them having $n_k^\ddagger$ transition states (being $n_1^\ddagger + \ldots + n_K^\ddagger = n^\ddagger$), we write the harmonic MP-TST rate constant, $k_{\mathrm{har}}^{\mathrm{MP-TST}}(T)$ as the sum over the TST rate constants of each channel

$$k_{\mathrm{har}}^{\mathrm{MP-TST}}(T) = \sum_{k=1}^{K} \tilde{k}_{\mathrm{har},k}^{\mathrm{TST}}(T), \tag{25}$$

where

$$\tilde{k}_{\mathrm{har},k}^{\mathrm{TST}}(T) = B(T) e^{-\beta V_k^\ddagger} \frac{\tilde{Q}_{\mathrm{har},k}^\ddagger}{\tilde{Q}_{\mathrm{har,R}}}, \tag{26}$$

being $\tilde{Q}^{\ddagger}_{\mathrm{har},k}$ the multi-conformational partition function of the kth CRC; $V^{\ddagger}_{k}$ is the difference in energy between the lowest energy transition state and the lowest energy transition state of the kth CRC. The TST rate constant of each of the CRCs can also be decomposed into a sum over the individual transition states ($i_k = 1, \ldots, n^{\ddagger}_{k}$) that belong to the kth CRC, i.e.,

$$\tilde{k}^{\mathrm{TST}}_{\mathrm{har},k}(T) = \sum_{i_k=1}^{n^{\ddagger}_{k}} k^{\mathrm{TST}}_{\mathrm{har},i_k}(T), \tag{27}$$

where

$$k^{\mathrm{TST}}_{\mathrm{har},i_k}(T) = B(T) e^{-\beta V^{\ddagger}_{k}} \frac{Q^{\mathrm{RRHO},\ddagger}_{i_k}}{\tilde{Q}_{\mathrm{har,R}}} \tag{28}$$

being

$$Q^{\mathrm{RRHO},\ddagger}_{i_k} = Q^{\ddagger}_{\mathrm{rot},i_k} Q^{\mathrm{HO},\ddagger}_{i_k} e^{-\beta U^{\ddagger}_{i_k}}. \tag{29}$$

The RRHO partition function of Eq. (29) is similar to that of Eq. (3), but for the i_kth transition state.

All the thermal rate constants from Eqs. (24) to (29) can be calculated just with electronic structure information (energies, geometries, and Hessians) of the reactants and the transition states. The calculation of the recrossing and quantum effects requires a deeper knowledge of the potential energy surface. Thus, the calculation of the CVT/LAT thermal rate constants involves the evaluation of the minimum energy path, as well as a wide region of the potential energy surface far from the minimum energy path called the reaction "swath." The calculation of these corrections is carried out for each of the transition states, and, therefore, we can define multiplicative coefficients of the type

$$\gamma^{\mathrm{CVT/LAT}}_{i_k} = \Gamma^{\mathrm{CVT}}_{i_k} \kappa^{\mathrm{CVT/LAT}}_{i_k}. \tag{30}$$

The substitution of Eq. (30) into Eq. (27) leads to the CVT/LAT thermal rate constant of the kth CRC, i.e.,

$$\tilde{k}^{\mathrm{CVT/LAT}}_{\mathrm{har},k}(T) = \sum_{i_k=1}^{n^{\ddagger}_{k}} \gamma^{\mathrm{CVT/LAT}}_{i_k} k^{\mathrm{TST}}_{\mathrm{har},i_k}(T). \tag{31}$$

An average of the recrossing and tunneling effects for each CRC can be obtained by dividing Eq. (31) by Eq. (27)

$$\langle \gamma \rangle^{\mathrm{CVT/LAT}}_{k} = \frac{\sum_{i_k=1}^{n^{\ddagger}_{k}} \gamma^{\mathrm{CVT/LAT}}_{i_k} Q^{\ddagger}_{\mathrm{rot},i_k} Q^{\mathrm{HO},\ddagger}_{i_k} e^{-\beta U^{\ddagger}_{i_k}}}{\tilde{Q}^{\ddagger}_{\mathrm{har},k}}. \tag{32}$$

The next step is to include torsional anharmonicity into the harmonic thermal rate constants. In the case of the multi-structural methods,[21] the torsional anharmonicity depends on the conformer, because the torsional potential energy surface is approximated by expansions of the potential about each stationary point. The 2D-NS method considers the global torsional potential of a given CRC. This global potential is used to solve the two-dimensional Schrödinger equation, leading to just one anharmonic parameter $\alpha^{\ddagger}_{\mathrm{tor},k}$ for each CRC. In principle, it would be possible to calculate the torsional anharmonicity of each of the transition states by defining torsional angle ranges for each conformer in a similar way as reported by Sturdy and Clary.[39] However, this treatment is out of the scope of this study and we concentrate on the torsional anharmonicity of each CRC, which is given by the ratio

$$\alpha_{\mathrm{tor},k} = \frac{\alpha^{\ddagger}_{\mathrm{tor},k}}{\alpha_{\mathrm{tor,R}}}, \tag{33}$$

where $\alpha_{\mathrm{tor,R}}$ is the anharmonic contribution due to reactants. It is possible to write the thermal rate constant for the kth CRC in a compact form of the type

$$\tilde{k}^{\mathrm{Y}}_{\mathrm{X},k}(T) = B(T) e^{-\beta V^{\ddagger}_{k}} \langle \gamma \rangle^{\mathrm{Y}}_{k} \alpha_{\mathrm{X},k} \frac{\tilde{Q}^{\ddagger}_{\mathrm{har},k}}{\tilde{Q}_{\mathrm{har,R}}} = \langle \gamma \rangle^{\mathrm{Y}}_{k} \alpha_{\mathrm{X},k} \tilde{k}^{\mathrm{TST}}_{\mathrm{har},k}(T), \tag{34}$$

where X = har *or* tor indicates harmonic or anharmonic treatment for torsional modes, and Y = TST or CVT/LAT. The harmonic thermal rate constant involves $\alpha_{\mathrm{har},k} = 1$. The multi-path thermal rate constant is given by

$$k^{\mathrm{MP-Y}}_{\mathrm{X}}(T) = \sum_{k=1}^{K} \tilde{k}^{\mathrm{Y}}_{\mathrm{X},k}(T). \tag{35}$$

In summary, the procedure to calculate $k^{\mathrm{MP-CVT/LAT}}_{\mathrm{tor}}(T)$ for a reaction with two torsions is the following:

(i) Locate all the n_{C} conformers of reactants.
(ii) Calculate $\tilde{Q}_{\mathrm{har,R}}$, i.e., the multi-conformational partition function of reactants.
(iii) Perform the scan over the two torsions and fit the data to the Fourier series of Eq. (10).
(iv) Calculate $Q^{\mathrm{2D-NS}}_{\mathrm{tor,R}}$ of Eq. (14).
(v) Evaluate $\overline{\omega}_{i,\tau}$, ($\tau$ = 1, 2) from Eq. (7) and calculate $\overline{Q}^{\mathrm{MC-HO}}_{\mathrm{tor,R}}$; use Eq. (4) and Eq. (1) to obtain $\alpha_{\mathrm{tor,R}}$ and $\tilde{Q}^{\mathrm{MD}}_{\mathrm{tor,R}}$, respectively.
(vi) Locate all the $n^{\ddagger}_{k}$ transition states of each CRCs, i.e., locate all the $n^{\ddagger}$ transition states.
(vii) Repeat steps (ii)-(v) for each of the CRCs.
(viii) Calculate $k^{\mathrm{MP-TST}}_{\mathrm{har}}(T)$ and $k^{\mathrm{MP-TST}}_{\mathrm{tor}}(T)$ for comparison.
(ix) For each transition state i_k calculate the individual $\gamma^{\mathrm{CVT}}_{i_k}$ and $\kappa^{\mathrm{CVT/LAT}}_{i_k}$ coefficients.
(x) Evaluate all the $\langle \gamma \rangle^{\mathrm{CVT/LAT}}_{k}$ coefficients and all the $\tilde{k}^{\mathrm{CVT/LAT}}_{\mathrm{X},k}(T)$ thermal rate constants.
(xi) Calculate $k^{\mathrm{MP-CVT/LAT}}_{\mathrm{har}}(T)$ and $k^{\mathrm{MP-CVT/LAT}}_{\mathrm{tor}}(T)$ thermal rate constants from Eq. (35).

For the calculation of the harmonic MP-CVT/LAT thermal rate constant only the steps (i), (ii), (vi), (viii)-(xi) are needed.

C. Computational details

All the electronic structure calculations were performed with Gaussian03[40] at the multi-coefficient three-parameters Becke88-Becke95 (MC3BB) method,[41] as for the hydrogen abstraction reaction from methanol by atomic hydrogen.[42] The torsional potential energy surfaces for ethanol and for each of the CRCs were scanned with a stepsize of 10°, allowing optimization of all geometric variables with the exception of the two dihedral angles that are specified at the beginning of Sec. III. For more details about the computation

of the torsional partition function, we refer to Ref. 14. The anharmonic coefficients of Eq. (4) were calculated with the HR2D program.[43]

The variational and tunneling contributions of each of the individual reaction paths to the thermal rate constants were calculated by following the minimum energy path in mass-scaled Cartesian coordinates (mass-weighted Cartesian coordinates divided by the square root of an arbitrary scaling mass μ) by the Page-McIver algorithm[44] using a stepsize of 0.005 a_0 and the scaling mass $\mu = 1$ amu. Hessians were calculated each 9 steps. The harmonic vibrational normal-mode frequencies along the minimum energy path were obtained using redundant internal coordinates.[45] The normal-mode frequencies were scaled by a factor of 0.979.[41] The LAT transmission coefficients were obtained using a double-interpolation scheme.[37] All the CVT/LAT calculations were performed using modified versions of POLYRATE[46] and GAUSSRATE9.7[47] programs. The latter was used as link between POLYRATE and Gaussian03 programs. The calculations to obtain the multi-conformational partition functions and the multi-path thermal rate constants were performed by the CONFORATE program.[48]

III. RESULTS AND DISCUSSION

The two torsions, which were scanned to generate the potentials of Eq. (10), are the H–O–C–C (ϕ_1) and the O–C–C–H (ϕ_2) dihedral angles, respectively. The coefficients of the Fourier series are given in the supplementary material.[49] For the definition of ϕ_2 in the reactants and the transition states of reactions (R1) and (R3), we have arbitrarily chosen one of the hydrogen atoms of the methyl group. In the case of the transition states of reaction (R2), the hydrogen atom taken as reference is the one being abstracted. Specifically, to unambiguously identify the stationary points, we have considered that a given atom (or group of atoms) is in alternate position (t) when the dihedral angles are in the interval [160°, 200°], and in gauge (g^+) and (g^-) positions when the dihedral angles are in the intervals [40°, 80°] and [280°, 320°], respectively. Ethanol presents three minima obtained by rotation about the ϕ_1 dihedral angle; the slightly most stable structure by 0.10 kcal/mol corresponds to the hydrogen of the OH group in alternate position with respect to the methyl group (**R**-t-t). The other two structures are enantiomers (and therefore isoenergetic), and correspond to the gauge dispositions of the hydroxylic hydrogen (**R**-g^+-t and **R**-g^--t). Newman projections and energetics of the reactants and the transition states are given in Fig. 1.

The geometries and normal-mode harmonic frequencies of the stationary points are listed in the supplementary material.[49] Table I lists the energetics of each of the transition states, which are classified by CRCs. The torsional potentials of ethanol and of each of the CRCs are given in Fig. 2. The energetic barriers of interconversion between the conformers of ethanol and between the conformers of the transition states of each CRC are also given in the supplementary material.[49] It should be noticed that all the torsional barriers for ethanol are much smaller than the barrier heights for hydrogen abstraction. Therefore, the rate constants of interconversion between conformers are larger than those for reaction. Under these conditions TST assumes that the equilibrium between the different conformations of the reactants is maintained. The same circumstance occurs for the interconversion between the products within a given CRC. However, the VTST formalism does not need accurate information about the interconversion barriers between different conformations of the products.

As expected, the hydrogen abstraction reaction from ethanol is more favorable when it occurs from a secondary carbon, and corresponds to transition state structures **TS1**-t-t, and its enantiomer **TS4**-t-t. The latter cannot be obtained from the former by internal rotations. Thus, reaction (R1) leads to two CRCs, i.e., **TS1** and **TS4**. This is because all the transition state structures of **TS1** that have enantiomers in **TS4** cannot interconvert by rotation about ϕ_1 and/or ϕ_2. In fact, the hindered rotor two-dimensional surfaces of **TS1** and **TS4** are specular images of each other. A given geometry with dihedral angles [ϕ_1, ϕ_2] in **TS1** corresponds to a geometry with dihedral angles [$360 - \phi_1$, $360 - \phi_2$] in **TS4**. It should be noticed that **TS1** and **TS4** also lead to different products, i.e., the products of **TS1** are enantiomers to those of **TS4**, but again they cannot interconvert between them because the hydrogen abstraction generates an asymmetric carbon. In general, the hydrogen abstraction from a molecule with a secondary carbon (for instance, R–CH_2–R′, being R and R′ two different groups), leads always to two CRCs with identical thermal rate constants. Thus, the thermal rate constant obtained for reaction (R1), since we are considering the formation of the CH_3CHOH radical in any conformation, is twice that obtained for **TS1**. Reactions (R2) and (R3) correspond each of them to one CRC, called **TS2** ($k = 2$) and **TS3** ($k = 3$), respectively. The former has 9 distinguishable transition states, whereas the latter has only 3. Within the same CRC, for the species that have two enantiomers (Table I), it is possible to include just one of them and to multiply the RRHO partition function of Eq. (29) by two.[22] The symmetry number for internal rotation about ϕ_2 (the rotation of the methyl group), $\sigma_{\mathrm{tor},2}$, is always three with the exception of **TS2**, which is the unity, because the hydrogen abstraction breaks the symmetry of the methyl group. The symmetry number for internal rotation about ϕ_1, $\sigma_{\mathrm{tor},1}$, is always the unity.

Fig. 3 shows the variation of the anharmonic coefficient α_{tor} with temperature. As indicated in Eq. (4) the coefficient α_{tor} represents the ratio between the full two-dimensional non-separable hindered rotor partition function and the multi-conformer harmonic oscillator partition function for the two torsions. It should be noticed that the torsional frequencies, $\overline{\omega}_{i,\tau}$ ($\tau = 1, 2$), may not coincide with the two normal-mode frequencies that are chiefly assigned to the torsions. At low temperatures, the value of α_{tor} for ethanol and for the four CRCs is larger than the unity. In all cases, α_{tor} reaches a maximum (ethanol has the maximum at about 250 K) and then decreases. At low temperatures, the density of states of the 2D-NS partition function increases faster than that of the MC-HO partition function, but as temperature increases the space explored by the hindered rotor partition function is larger and the density of states of 2D-NS increases slowly than that of MC-HO. In any case, the values of $\alpha_{\mathrm{tor},k}$ that are given by Eq. (33) are smaller, although quite close to unity, for the four CRCs

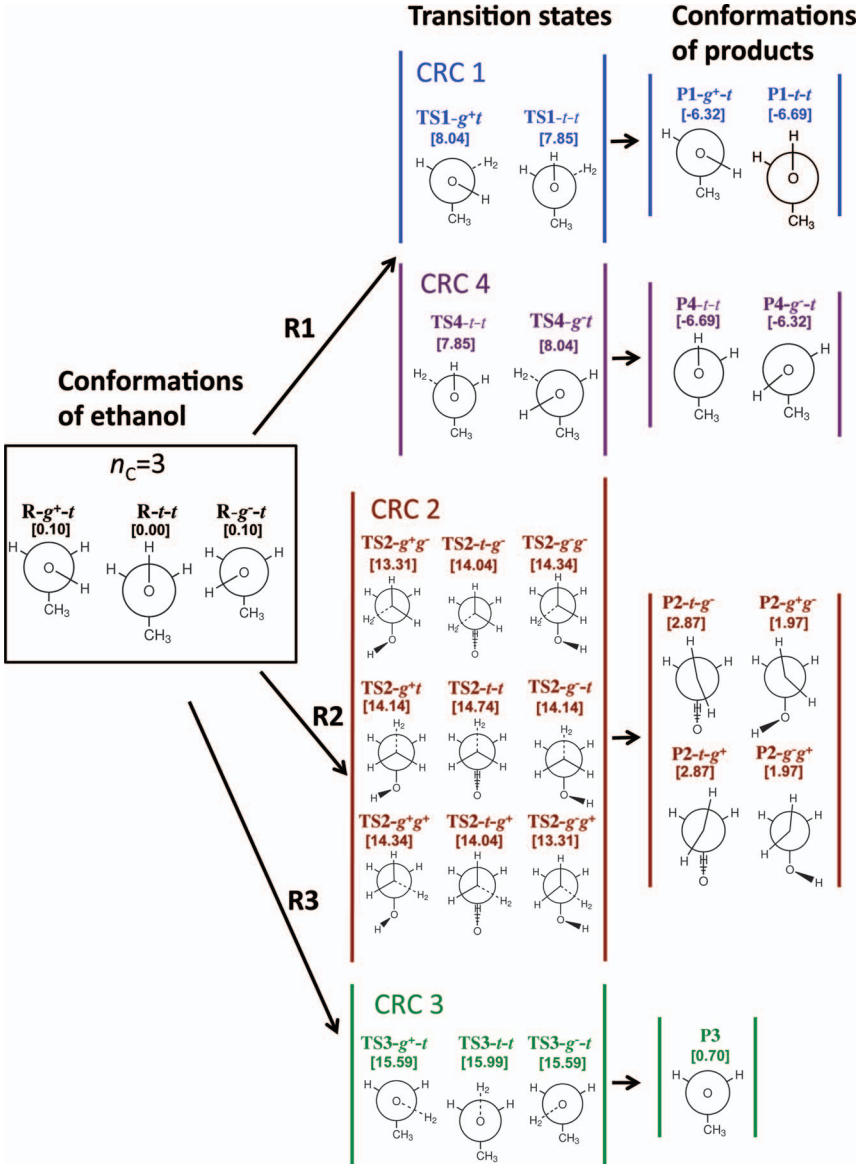

FIG. 1. Scheme that shows the three hydrogen abstraction reactions and the four conformational reaction channels associated to them, together with all the conformations of reactants, transition states, and products. Newman projections, as well as the name of the conformers and the relative energies (in kcal/mol), are also indicated.

TABLE I. Energetics (in kcal mol^{-1}) of all the transition states for reaction including enantiomers. In all cases, $V_0^{\ddagger} = 7.85$ kcal mol^{-1}. Notice that $V_{i_k}^{\ddagger} = V_0^{\ddagger} + V_k^{\ddagger} + U_{i_k}^{\ddagger}$.

Conformer	$V_k^{\ddagger}$	$U_{i_k}^{\ddagger}$	$V_{i_k}^{\ddagger}$
TS1-*t*-*t*		0.00	7.85
TS1-g^+-*t*	0.00	0.19	8.04
TS4-*t*-*t*		0.00	7.85
TS4-g^--*t*	0.00	0.19	8.04
TS2-g^--g^+, **TS2**-g^+-g^-		0.00	13.31
TS2-*t*-g^+, **TS2**-*t*-g^-		0.73	14.04
TS2-g^--*t*, **TS2**-g^+-*t*	5.46	0.83	14.14
TS2-g^--g^-, **TS2**-g^+-g^+		1.03	14.34
TS2-*t*-*t*		1.43	14.74
TS3-g^+-*t*,**TS3**-g^--*t*		0.00	15.59
TS3-*t*-*t*	7.74	0.40	15.99

at temperatures below 500 K (Table II). However, above that temperature, with the exception of $\alpha_{\text{tor},2}$, which remains very close to unity, the torsional anharmonicity increases the value of the thermal rate constants. The overall effect of the torsional anharmonicity in the range of temperatures studied is that increases the slope of the Arrhenius plot with respect to the harmonic values.

Table II also lists the $\langle\gamma\rangle_k^{\text{CVT/LAT}}$ coefficients for the four CRCs. These coefficients average the recrossing and tunneling contributions to the TST thermal rate constants of each CRC (i.e., they measure the deviations from conventional TST). It should be noticed that $\langle\gamma\rangle_k^{\text{CVT/LAT}}$ is given by Eq. (32), which is different from the average of the individual values $\gamma_{i_k}^{\text{CVT/LAT}}$ of each reaction path. The individual values are listed in the supplementary material.[49] Because we are studying hydrogen abstraction reactions, the main contribution to $\langle\gamma\rangle_k^{\text{CVT/LAT}}$ at low temperatures is due to tunneling.

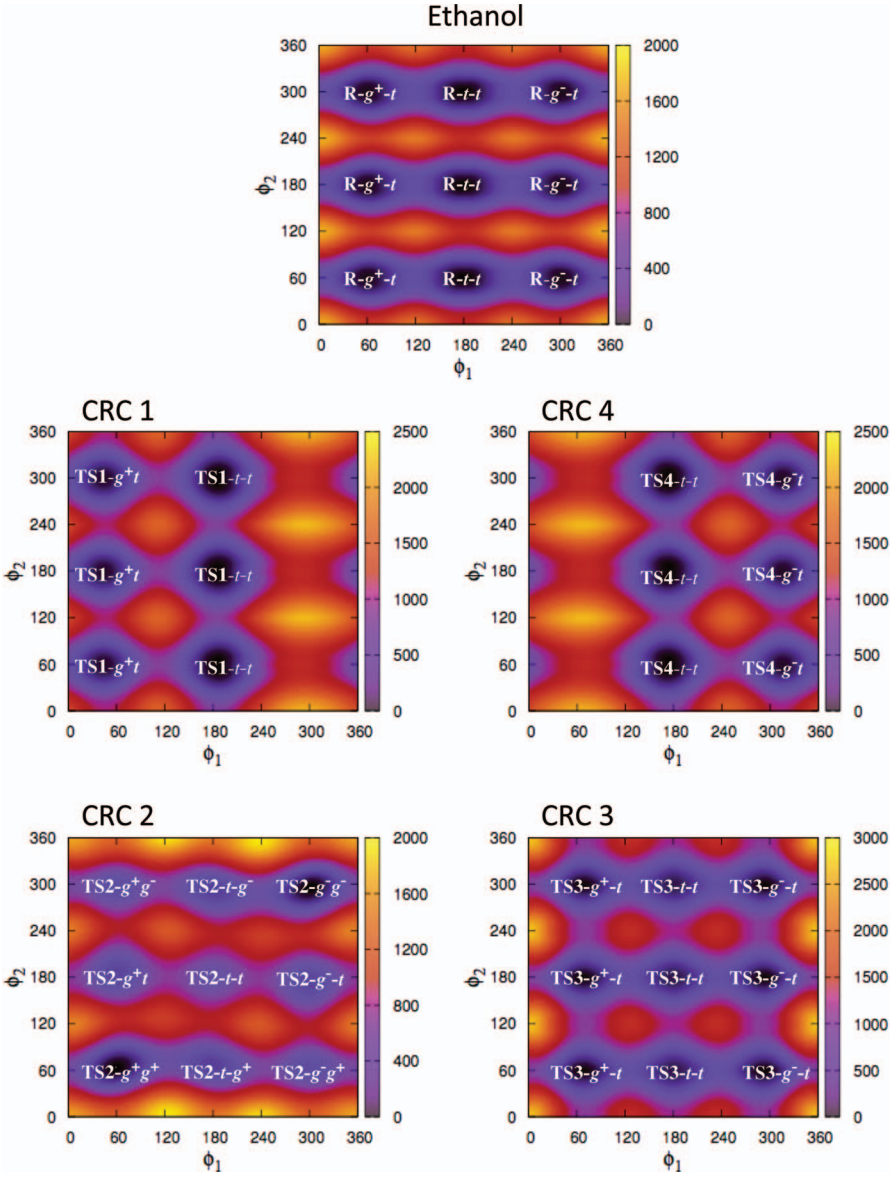

FIG. 2. Color contour plots of the energy landscapes (in cm^{-1}) resulting from the internal rotation of ethanol and the four CRCs; ϕ_1 is about the H–O–C–C torsion, and ϕ_2 is about the O–C–C–H torsion (in the case of CRC2 the hydrogen atom refers to the one being abstracted). Those minima with the same label refer to indistinguishable conformations.

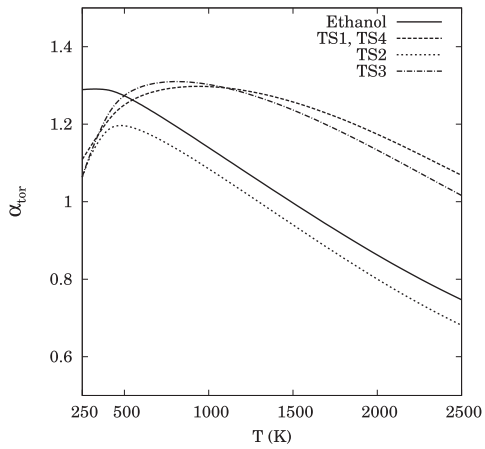

FIG. 3. Anharmonic torsional coefficient α_{tor} for the four CRCs calculated from Eq. (4).

In fact, the TST thermal rate constants are substantially increased by this quantum effect. Thus, at room temperature tunneling increases the reaction rates of (R1)–(R3) by factors of 6.9, 7.3, and 16.0, respectively, although for (R2) and (R3) the variational effects at room temperature decrease the thermal rate constants by factors of 0.80 and 0.55, respectively. Due to the energy differences between reaction (R1) and the other hydrogen abstraction reactions, the total thermal rate constant is completely dominated by (R1) at low temperatures (Table III), although at temperatures above 1000 K the other two channels start to contribute [Fig. 4]. Norton and Dryer,[1] and Marinov[3] reported branching ratios of 50:30:20 and 54:26:20, respectively, for R1:R2:R3 at $T = 1100$ K. However, our calculations indicate that the contribution of the two channels with the highest energy is more modest, i.e., 15% and 2% for (R2) and (R3), respectively. Figure 4 also shows that torsional anharmonicity has some

TABLE II. Multiplicative coefficients to the harmonic TST thermal rate constant of Eq. (26) of the kth CRC (columns 2-7) to obtain the corresponding CVT/LAT thermal rate constant of the rhs of Eq. (35). The last two columns list the multiplicative coefficients to obtain the MP-CVT anharmonic thermal rate constants from the harmonic MP-TST values.

T(K)	$\langle\gamma\rangle_{1,4}^{\mathrm{CVT/LAT}}$	$\alpha_{\mathrm{tor},1,4}$	$\langle\gamma\rangle_{2}^{\mathrm{CVT/LAT}}$	$\alpha_{\mathrm{tor},2}$	$\langle\gamma\rangle_{3}^{\mathrm{CVT/LAT}}$	$\alpha_{\mathrm{tor},3}$	$\langle\gamma\rangle^{\mathrm{CVT/LAT}}$	$\alpha_{\mathrm{tor,t}}$
250.0	21.39	0.860	19.44	0.825	47.76	0.825	21.39	0.860
298.2	6.86	0.885	5.78	0.871	8.79	0.873	6.86	0.885
390.2	2.64	0.933	2.29	0.923	2.47	0.947	2.64	0.933
423.2	2.22	0.950	1.96	0.934	2.01	0.969	2.22	0.937
479.2	1.82	0.979	1.64	0.946	1.61	1.002	1.82	0.979
500.0	1.72	0.990	1.56	0.949	1.51	1.013	1.72	0.990
1000.0	1.12	1.201	1.07	0.961	1.02	1.200	1.11	1.166
2000.0	1.01	1.383	0.98	0.925	0.95	1.288	1.00	1.188
2500.0	0.99	1.430	0.98	0.919	0.94	1.360	0.98	1.173

effect on the branching ratios, i.e., increases the percentage of reaction (R1) that raises from 45% to 54% at $T = 2500$ K at the expense of reaction (R2).

The total MP-CVT/LAT thermal rate constant is given by

$$\begin{aligned} k_{\mathrm{tor}}^{\mathrm{MP-CVT/LAT}}(T) &= \sum_{k=1}^{4} \tilde{k}_{\mathrm{tor},k}^{\mathrm{CVT/LAT}}(T) \\ &= 2\tilde{k}_{\mathrm{tor},1}^{\mathrm{CVT/LAT}}(T) + \tilde{k}_{\mathrm{tor},2}^{\mathrm{CVT/LAT}}(T) + \tilde{k}_{\mathrm{tor},3}^{\mathrm{CVT/LAT}}(T). \end{aligned} \quad (36)$$

The factor of two is due to the fact that **TS1** and **TS4** are specular images.

The anharmonic CVT/LAT thermal rate constants of each CRC were fitted to the following equation:[50]

$$k(T) = A\left(\frac{T}{300}\right)^{n} \exp\left[\frac{-E(T+T_0)}{T^2+T_0^2}\right]. \quad (37)$$

This equation has four fitting parameters: A, n, T_0, and E. The errors in the fitting were calculated as the value of the root mean square residual (RMSR), which is given by

$$\mathrm{RMSR} = \left\{\frac{1}{N}\left[\sum_{i=1}^{N} \ln\left(\frac{k(T_i)}{k_M(p_1,\ldots,p_K,T_i)}\right)\right]^2\right\}^{1/2}, \quad (38)$$

where N is the number of temperatures, which in this case were 13 temperatures in the interval 250-2500 K; $k(T_i)$ is the CVT/LAT thermal rate constant at T_i, and $k_M(p_1, \ldots, p_K, T_i)$ are the fitted thermal rate constants involving the K parameters given by Eq. (37) (in this case $K = 4$). The fitting parameters are listed in Table IV. Equation (37) is very useful to obtain activation energies, E_a, in a wide range of temperatures

$$E_a = E\frac{T^4 + 2T_0T^3 - T_0^2T^2}{(T^2+T_0^2)^2} + nRT. \quad (39)$$

The activation energy for the total abstraction reaction varies from 2.82 kcal/mol at $T = 250$ K to 18.11 kcal/mol at $T = 2500$ K. Aders and Wagner[5] fitted their experimental thermal rate constants to the Arrhenius equation

$$k(T) = A\exp\left[\frac{-E_a}{RT}\right] \quad (40)$$

in the interval of temperatures between 295 and 700 K. They obtained an activation energy of 2.11 ± 0.15 kcal/mol. In the same interval of temperatures, we obtained a variation of the activation energy between 3.57 and 7.76 kcal/mol. Clearly, the use of the Arrhenius equation in these circumstances is inadequate and, as it is shown in Fig. 5, the slope of the straight line given by Aders and Wagner[5] is too small. However, our MP-CVT/LAT calculations including torsional anharmonicity for the total rate constant agree very well with the

TABLE III. Anharmonic MP-CVT/LAT thermal rate constants for (R1) (**TS1**+**TS4** CRCs), (R2) and (R3), and for the total hydrogen abstraction process (columns 2-5). Experimental rate constants are listed in column 6. The TST and the harmonic thermal rate constants can be obtained combining this table with Table II. All rate constants are in cm^3 molecule^{-1} s^{-1}.

T(K)	$\tilde{k}_{\mathrm{tor},1+4}^{\mathrm{CVT/LAT}}$	$\tilde{k}_{\mathrm{tor},2}^{\mathrm{CVT/LAT}}$	$\tilde{k}_{\mathrm{tor},3}^{\mathrm{CVT/LAT}}$	$k_{\mathrm{tor}}^{\mathrm{MP-CVT/LAT}}$	Exp.[a]
250.0	9.30×10^{-16}	1.92×10^{-20}	4.85×10^{-22}	9.30×10^{-16}	...
298.2	2.48×10^{-15}	3.15×10^{-19}	8.50×10^{-21}	1.75×10^{-15}	5.8×10^{-15}
390.2	1.38×10^{-14}	1.84×10^{-17}	6.78×10^{-19}	1.39×10^{-14}	3.1×10^{-14}
423.2	2.34×10^{-14}	5.68×10^{-17}	2.35×10^{-18}	2.35×10^{-14}	4.7×10^{-14}, 2.2×10^{-14}
479.2	5.15×10^{-14}	2.85×10^{-16}	1.41×10^{-17}	5.18×10^{-14}	8.5×10^{-14}
500.0	6.70×10^{-14}	4.81×10^{-16}	2.53×10^{-17}	6.76×10^{-14}	1.2×10^{-13}
1000.0	2.66×10^{-12}	3.46×10^{-13}	4.02×10^{-14}	3.04×10^{-12}	...
2000.0	3.82×10^{-11}	1.99×10^{-11}	3.57×10^{-12}	6.16×10^{-11}	...
2500.0	7.66×10^{-11}	5.22×10^{-11}	1.03×10^{-11}	1.39×10^{-10}	...

[a]Experimental values from Refs. 5 and 6 (second value at $T = 423.2$ K).

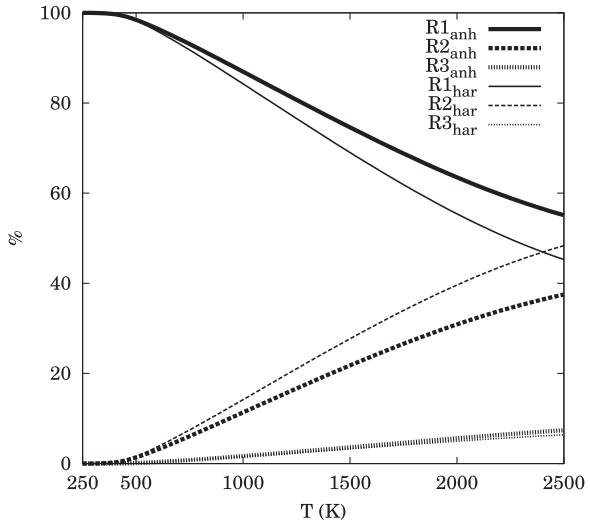

FIG. 4. Branching ratios obtained from the harmonic (har) and anharmonic (anh) MP-CVT/LAT calculations expressed as percentage: $\%_{Ri} = \frac{k_{Ri}}{\sum_{i=1}^{3} k_{Ri}}$.

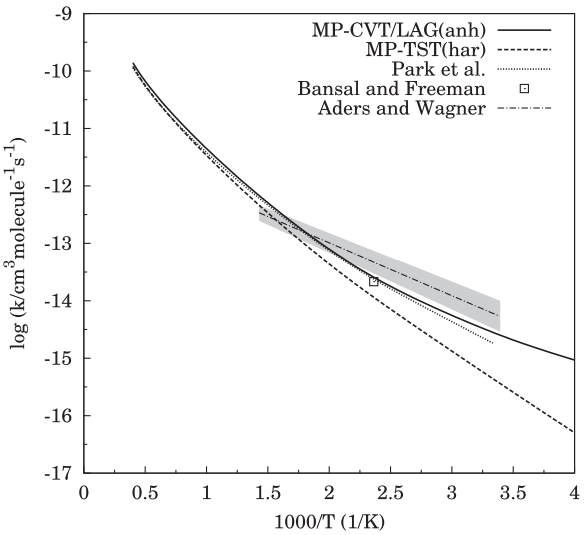

FIG. 5. Arrhenius plot showing the MP-CVT/LAT (with anharmonic corrections) and the MP-TST (harmonic) thermal rate constants. The previous calculations by Park *et al.*[7] and the experimental data by Bansal and Freeman[6] and by Aders and Wagner[5] (the gray area indicates the error bars) are also shown.

experiment of γ radiolysis carried out by Bansal and Freeman[6] at $T = 423.2$ K.

The interconversion between the reactants is much faster than the hydrogen abstraction reactions, so all of the conformers contribute to each of the transition states. Although we cannot validate the individual rates, if we want to calculate the percentage of molecules that pass through each of the transition states, TST tells us that for each CRC, this percentage is given by the ratio

$$P_{i_k}^{\mathrm{TST}}(T) = \frac{k_{\mathrm{har},i_k}^{\mathrm{TST}}(T)}{\tilde{k}_{\mathrm{har},k}^{\mathrm{TST}}(T)} \times 100 = \frac{Q_{i_k}^{\mathrm{RRHO},\ddagger}}{\tilde{Q}_{\mathrm{har},k}^{\ddagger}} \times 100$$

$$= \frac{G_{i_k}^{\ddagger,\mathrm{o}}}{\sum_{i_k=1}^{n_k^{\ddagger}} G_{i_k}^{\ddagger,\mathrm{o}}} \times 100, \tag{41}$$

where the last part of the rhs of Eq. (41) is written as a function of standard-state free energy of the i_kth transition state, $G_{i_k}^{\ddagger,\mathrm{o}}$, instead of as a function of partition functions. For the case of two reactants in fast interconversion and two transition states, this is known as the Curtin-Hammett principle,[51] which is widely applied in Organic Chemistry. It states that the relative rate constants of the process depend only on the transition state free energies. The application of this principle to **TS1**, which has two distinguishable transition states **TS1**-*t*-*t* (i=1), and **TS1**-g^+-*t* (i=2), shows that the percentage of molecules that cross through the dividing surface at **TS1**-*t*-*t* is given by

$$P_{1_1}^{\mathrm{TST}}(T) = \frac{1}{1 + \frac{G_{2_1}^{\ddagger,\mathrm{o}}}{G_{1_1}^{\ddagger,\mathrm{o}}}} \times 100 \tag{42}$$

whereas the ones that cross through the dividing surface at **TS1**-g^+-*t* are

$$P_{2_1}^{\mathrm{TST}}(T) = 100 - P_{1_1}^{\mathrm{TST}}(T). \tag{43}$$

At room temperature, **TS1**-*t*-*t* contributes 61% to the total flux toward products, whereas **TS1**-g^+-*t* only 39%. These percentages change to 53% and 47% for **TS1**-*t*-*t* and **TS1**-g^+-*t*, respectively, at $T = 2500$ K. Therefore, even in conventional MP-TST, the temperature affects the forward flux through each of the transition states, since higher temperatures favor the most energetic saddle points. As a consequence, the incorporation of multiple paths into the thermal rate constants has a different effect than if just one transition state is been considered. There is an additional and more important factor that justifies the incorporation of multiple paths into the evaluation of thermal rate constants in reactions as the

TABLE IV. Fitting parameters to the CVT/LAT thermal rate constants obtained for (R1)–(R3), and to the MP-CVT thermal rate constant ((R1) + (R2) + (R3)) using Eq. (37). The RMSR values are also given.

	Reaction			
Parameter	(R1) + (R2) + (R3)	(R1)	(R2)	(R3)
A (cm^3 s^{-1}molecule^{-1})	5.180×10^{-13}	1.611×10^{-12}	1.391×10^{-13}	3.506×10^{-13}
n	2.948	2.193	2.488	2.502
E (K)	1487	1801	3856	4488
T_0 (K)	261.1	258.3	170.9	191.8
RMSR	0.018	0.014	0.010	0.015

TABLE V. Ratios between the anharmonic MP-CVT/LAT thermal rate constants for the overall hydrogen abstraction process and the following: the rate constants calculated by Park *et al.*,[7] k_{Park}; and the harmonic MP-CVT/LAT rate constants considering only the lowest energy transition states of **TS1**, **TS2**, and **TS3**, and the most stable reactant, k_{approx1}, or considering all reactant conformations, k_{approx2}.

T(K)	$\frac{k_{\text{tor}}^{\text{MP-CVT/LAT}}}{k_{\text{Park}}}$	$\frac{k_{\text{tor}}^{\text{MP-CVT/LAT}}}{k_{\text{approx1}}}$	$\frac{k_{\text{tor}}^{\text{MP-CVT/LAT}}}{k_{\text{approx2}}}$
250.0	...	2.15	5.25
298.2	1.45	1.57	3.86
390.2	1.05	1.32	3.39
423.2	1.01	1.31	3.37
479.2	1.00	1.33	3.48
500.0	1.00	1.34	3.52
1000.0	1.15	1.70	4.61
2000.0	1.26	2.13	5.87
2500.0	1.22	2.24	6.21

one studied here. The results from Eqs. (42) and (43) are exclusively based on transition state properties. However, MP-TST is not adequate for hydrogen transfer reactions, because it ignores quantum effects, and they are relevant at low temperatures. The MP-CVT/LAT methodology includes recrossing and quantum effects, so the contribution of the individual transition states to each CRC is given by

$$P_{i_k}^{\text{CVT/LAT}}(T) = \frac{k_{\text{har},i_k}^{\text{CVT/LAT}}(T)}{\tilde{k}_{\text{har},k}^{\text{CVT/LAT}}(T)} \times 100 = \frac{\gamma_{i_k}^{\text{CVT/LAT}}}{\langle\gamma\rangle_k^{\text{CVT/LAT}}} P_{i_k}^{\text{TST}}(T). \tag{44}$$

The value of $\gamma_{1_1}^{\text{CVT/LAT}}$ (of the **TS1**-*t*-*t* conformer) is 5.15 at room temperature, whereas the value of $\gamma_{2_1}^{\text{CVT/LAT}}$ is 9.18. These two values revert the TST-based contributions of the two transition states to the **TS1** thermal rate constant, which are now 46% and 54% for **TS1**-*t*-*t* and **TS1**-g^+-*t*, respectively. At $T = 2500$ K, the percentages are basically the same as for MP-TST, since tunneling is negligible at high temperatures. Therefore, the incorporation of tunneling into each of the reaction paths increases the thermal rate constant with respect to single path calculations.

In this context, it is interesting to analyze the influence of multiple paths on the rate constants in relation to the single-path calculations carried out by other researchers.[7] The ratios between the anharmonic MP-CVT/LAT rate constants and the calculations by Park *et al.*[7] ($k_{\text{tor}}^{\text{MP-CVT/LAT}}/k_{\text{Park}}$) are listed in Table V. Their values agree very well with ours above room temperature, although their rate constants are somewhat lower at low and high temperatures. Those authors only included in their calculations the most stable conformation of ethanol and the lowest energy transition states of **TS1**, **TS2**, and **TS3**. Basically, they performed a single path VTST calculation for each of the CRCs. It is interesting to repeat this type of calculation, but at the MC3BB level ($k_{\text{tor}}^{\text{MP-CVT/LAT}}/k_{\text{approx1}}$ ratio in Table V), to have a more reliable indicator of MP-VTST versus single path VTST. In this way, we avoid compensation of errors derived from the differences in the level of the electronic structure calculations, the methodology to evaluate the tunneling contribution, and the anharmonic effects. If all calculations are performed at the same level of electronic structure, the ratios between MP-CVT/LAT and single-path CVT/LAT are 2.15 and 2.24 at $T = 250$ K and 2500 K, respectively. The ratios increase substantially when the calculation includes all the conformations of ethanol ($k_{\text{tor}}^{\text{MP-CVT/LAT}}/k_{\text{approx2}}$). Interestingly enough, the three ratios listed in Table V show the same temperature dependence, i.e., larger ratios (more influence of the multiple paths) at low and high temperatures. As we have pointed out in the previous paragraph, at low temperatures this is due to the tunneling effect, and at high temperatures to the larger contribution of high energy transition states. Therefore, an Arrhenius plot considering multiple paths will be more curved than that considering a single path.

The contribution of each of the transition states to the thermal rate constant and how this contribution is affected by tunneling may not seem too important in this case, because all the transition states of **TS1** lead to different conformations of the same product. However, this issue becomes very important when the transition states lead to different products, since in this case we may have a change in the mechanism of reaction. For instance, this occurs in the isomerization reaction of methylhydroxycarbene. At low temperatures, it isomerizes to acetaldehyde and at high temperatures to vinyl alcohol.[52] The former product goes through a higher barrier than the latter, but tunneling effect is more important in the case of the formation of acetaldehyde and compensates the difference in energy.

IV. CONCLUSION

In this work, we have investigated the hydrogen abstraction reaction of ethanol by atomic hydrogen by means of MP-VTST, to which we have added a novel method to account for torsional anharmonicity. The MP-VTST thermal rate constant, calculated with the CVT/LAT method, is defined as a sum over conformational reaction channels. Each of these reaction channels includes all the structures that can be reached by internal rotation. For this reaction, torsional anharmonicity enhances the slope of the Arrhenius plot with respect to the harmonic approximation. Both, the reactants and the transition states present conformational flexibility, but the MP-CVT/LAT method is able to include all the conformations of reactants, as well as all the possible reaction paths (including recrossing and tunneling corrections). In the interval of temperatures between 250 and 2500 K, if multiple paths are taken into account, the thermal rate constants increase with respect to the single path approach, mainly at low and at high temperatures. On the other hand, even if we are already using a multi-path formalism, the analysis based on transition state free energies may not be an adequate measure of the contribution of each of the transition states to the total thermal rate constant because of quantum effects.

[1] T. S. Norton and F. L. Dryer, Int. J. Chem. Kinet. **24**, 319 (1992).
[2] H. J. Curran, M. P. Dunphy, J. M. Simmie, C. K. Westbrook, and W. J. Pitz, Symp. (Int.) Combust. **24**, 769 (1992).
[3] N. M. Marinov, Int. J. Chem. Kinet. **31**, 183 (1999).
[4] J. Li, A. Kazarov, and F. L. Dryer, Int. J. Chem. Kinet. **33**, 859 (2001).
[5] W. K. Aders and H. G. Wagner, Ber. Bunsenges. Phys. Chem. **77**, 712 (1973).

[6]K. M. Bansal and G. R. Freeman, J. Am. Chem. Soc. **90**, 5632 (1968).
[7]J. Park, Z. F. Xu, and M. C. Lin, J. Chem. Phys. **118**, 9990 (2003).
[8]H. Eyring, J. Chem. Phys. **3**, 107 (1935).
[9]R. Meana-Pañeda and A. Fernández-Ramos, J. Am. Chem. Soc. **134**, 346 (2012); **134**, 7193 (2012) (Erratum).
[10]D. G. Truhlar, A. D. Isaacson, and B. C. Garrett, in *Theory of Chemical Reaction Dynamics*, edited by M. Baer (CRC, Boca Raton, FL, 1985), Vol. 4, p. 65.
[11]A. Fernández-Ramos, A. Ellingson, B. C. Garrett, and D. G. Truhlar, Rev. Comput. Chem. **23**, 125 (2007).
[12]T. Yu, J. Zheng, and D. G. Truhlar, J. Phys. Chem. A **116**, 297 (2012).
[13]J. Zheng and D. G. Truhlar, J. Chem. Theory Comput. **9**, 2875 (2013).
[14]A. Fernández-Ramos, J. Chem. Phys. **138**, 134112 (2013).
[15]T. F. Miller III and D. C. Clary, J. Chem. Phys. **116**, 8262 (2002).
[16]T. F. Miller III and D. C. Clary, J. Chem. Phys. **119**, 68 (2003).
[17]T. F. Miller III and D. C. Clary, Mol. Phys. **103**, 1573 (2005).
[18]Y. K. Sturdy and D. C. Clary, Phys. Chem. Chem. Phys. **9**, 2397 (2007).
[19]J. Zheng and D. G. Truhlar, J. Chem. Theory Comput. **9**, 1356 (2013).
[20]P. Vansteenkiste, D. Van Neck, V. Van Speybroeck, and M. Waroquier, J. Chem. Phys. **124**, 044314 (2006); **125**, 049902 (2006) (Erratum).
[21]J. Zheng, T. Yu, E. Papajak, I. M. Alecu, S. L. Mielke, and D. G. Truhlar, Phys. Chem. Chem. Phys. **13**, 10885 (2011).
[22]A. Fernández-Ramos, B. A. Ellingson, R. Meana-Pañeda, J. M. C. Marques, and D. G. Truhlar, Theor. Chem. Acc. **118**, 813 (2007).
[23]J. E. Kilpatrick and K. S. Pitzer, J. Chem. Phys. **17**, 1064 (1949).
[24]B. C. Garrett and D. G. Truhlar, J. Chem. Phys. **70**, 1593 (1979).
[25]B. C. Garrett and D. G. Truhlar, J. Phys. Chem. **83**, 1052 (1979).
[26]B. Kerkeni and D. C. Clary, J. Chem. Phys. **121**, 6809 (2004).
[27]B. Kerkeni and D. C. Clary, Phys. Chem. Chem. Phys. **8**, 917 (2006).
[28]T. C. Allison and D. G. Truhlar, in *Modern Methods for Multidimensional Dynamics Computations in Chemistry*, edited by D. L. Thompson (World Scientific, Singapore, 1998), p. 618.
[29]J. Pu and D. G. Truhlar, J. Chem. Phys. **117**, 1479 (2002).
[30]R. A. Marcus and M. E. Coltrin, J. Chem. Phys. **67**, 2609 (1977).
[31]D.-h. Lu, T. N. Truong, V. S. Melissas, G. C. Lynch, Y.-P. Liu, B. C. Garrett, R. Steckler, A. D. Isaacson, S. N. Rai, G. C. Hancock, J. G. Lauderdale, T. Joseph, and D. G. Truhlar, Comput. Phys. Commun. **71**, 235 (1992).
[32]Y.-P. Liu, G. C. Lynch, T. N. Truong, D.-h. Lu, and D. G. Truhlar, J. Am. Chem. Soc. **115**, 2408 (1993).
[33]A. Fernández-Ramos and D. G. Truhlar, J. Chem. Phys. **114**, 1491 (2001).
[34]B. C. Garrett and D. G. Truhlar, J. Chem. Phys. **79**, 4931 (1983).
[35]G. C. Lynch, D. G. Truhlar, and B. C. Garrett, J. Chem. Phys. **90**, 3102 (1989).
[36]R. Meana-Pañeda, D. G. Truhlar, and A. Fernández-Ramos, J. Chem. Theory Comput. **6**, 6 (2010).
[37]R. Meana-Pañeda, D. G. Truhlar, and A. Fernandez-Ramos, J. Chem. Theory Comput. **6**, 3015 (2010).
[38]R. Meana-Pañeda and A. Fernández-Ramos, in *Kinetics and Dynamics: From Nano- to Bio-Scale*, edited by P. Paneth and A. Dybala-Defratyka (Springer, Dordrecht, Germany, 2010), Vol. 12, p. 481.
[39]Y. K. Sturdy and D. C. Clary, Phys. Chem. Chem. Phys. **9**, 2065 (2007).
[40]M. J. Frisch, G. W. Trucks, H. B. Schlegel, *et al.*, Gaussian 03, Revision version B.05, Gaussian, Inc., Pittsburgh, PA, 2003.
[41]Y. Zhao, B. J. Lynch, and D. G. Truhlar, J. Phys. Chem. A **108**, 4786 (2004).
[42]R. Meana-Pañeda, D. G. Truhlar, and A. Fernández-Ramos, J. Chem. Phys. **134**, 094302 (2011).
[43]A. Fernández-Ramos, HR2D version 1.0, Universidade de Santiago de Compostela, Santiago de Compostela, 2012.
[44]M. Page and J. W. McIver, Jr., J. Chem. Phys. **88**, 922 (1988).
[45]Y. Y. Chuang and D. G. Truhlar, J. Phys. Chem. A **102**, 242 (1998).
[46]J. C. Corchado, Y.-Y. Chuang, P. L. Fast, W.-P. Hu, Y.-P. Liu, G. C. Lynch, K. A. Nguyen, C. F. Jackels, A. Fernández-Ramos, B. A. Ellingson, B. J. Lynch, J. Zheng, V. S. Melissas, J. Villa, I. Rossi, E. L. Coitiño, J. Pu, T. V. Albu, R. Steckler, B. C. Garrett, A. D. Isaacson, and D. G. Truhlar, POLYRATE−version 9.7, University of Minnesota, Minneapolis, 2007.
[47]J. C. Corchado, Y.-Y. Chuang, E. L. Coitiño, B. A. Ellingson, J. Zheng, and D. G. Truhlar, GAUSSRATE−version 9.7, University of Minnesota, Minneapolis, 2007.
[48]R. Meana-Pañeda and A. Fernández Ramos, CONFORATE−version 2.0, Universidade de Santiago de Compostela, Santiago de Compostela, 2013.
[49]See supplementary material at http://dx.doi.org/10.1063/1.4873350 for all the Cartesian coordinates, frequencies, and absolute energies of the stationary points; the internal rotation interconversion barriers between reactants and between the transition states of each CRC; the fitting parameters for the Fourier series of potential of Eq. (10); the relative energies, partition functions of all reactants and transition state structures, as well as all the individual TST and CVT/LAT thermal rate constants. The variational, tunneling, and anharmonic contributions and the percentage of contribution of each individual transition state to the CRC are also included. Finally, the total harmonic and anharmonic MP-TST and MP-CVT/LAT thermal rate constants and the branching ratios are also listed.
[50]J. Zheng and D. G. Truhlar, Phys. Chem. Chem. Phys. **12**, 7782 (2010).
[51]J. I. Seeman, Chem. Rev. **83**, 83 (1983).
[52]P. R. Schreiner, H. P. Reisenauer, D. Ley, D. Gerbig, C.-H. Wu, and W. D. Allen, Science **332**, 1300 (2011).